


## Article

# Property Analysis of Photo-Polymerization-Type 3D-Printed Structures Based on Multi-Composite Materials

So-Ree Hwang<sup>1</sup> and Min-Soo Park<sup>2,\*</sup> 

<sup>1</sup> Graduate School of NID Fusion Technology, Seoul National University of Science and Technology, 232 Gongneung-ro, Nowon-gu, Seoul 01811, Korea; zhengyin3216@naver.com

<sup>2</sup> Department of Mechanical System Design Engineering, Seoul National University of Science and Technology, Seoul 01811, Korea

\* Correspondence: pminsoo@seoultech.ac.kr; Tel.: +82-2-970-6356

**Abstract:** Additive manufacturing, commonly called 3D printing, has been studied extensively because it can be used to fabricate complex structures; however, polymer-based 3D printing has limitations in terms of implementing certain functionalities, so it is limited in the production of conceptual prototypes. As such, polymer-based composites and multi-material 3D printing are being studied as alternatives. In this study, a DLP 3D printer capable of printing multiple composite materials was fabricated using a movable separator and structures with various properties were fabricated by selectively printing two composite materials. After the specimen was fabricated based on the ASTM, the basic mechanical properties of the structure were compared through a 3-point bending test and a ball rebound test. Through this, it was shown that structures with various mechanical properties can be fabricated using the proposed movable-separator-based DLP process. In addition, it was shown that this process can be used to fabricate anisotropic structures, whose properties vary depending on the direction of the force applied to the structure. By fabricating multi-joint grippers with varying levels of flexibility, it was shown that the proposed process can be applied in the fabrication of soft robots as well.

**Keywords:** multi-composite materials; photo-polymerization; additive manufacturing; 3D printing; photochromic; laminar composite



**Citation:** Hwang, S.-R.; Park, M.-S. Property Analysis of Photo-Polymerization-Type 3D-Printed Structures Based on Multi-Composite Materials. *Appl. Sci.* **2021**, *11*, 8545. <https://doi.org/10.3390/app11188545>

Academic Editor: Joamin Gonzalez-Gutierrez

Received: 30 June 2021

Accepted: 8 September 2021

Published: 14 September 2021

**Publisher's Note:** MDPI stays neutral with regard to jurisdictional claims in published maps and institutional affiliations.



**Copyright:** © 2021 by the authors. Licensee MDPI, Basel, Switzerland. This article is an open access article distributed under the terms and conditions of the Creative Commons Attribution (CC BY) license (<https://creativecommons.org/licenses/by/4.0/>).

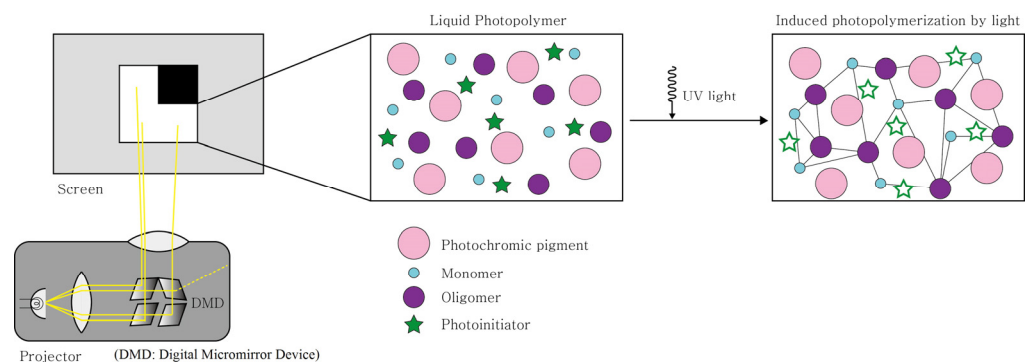
## 1. Introduction

The polymers used in 3D printers must have various material properties depending on the printing method, meaning there can be differences in resolution and surface quality. The various 3D printing methods using heat sources such as heat cartridges or lasers mainly use thermoplastic polymers such as acrylonitrile butadiene styrene (ABS) [1–3], polylactic acid (PLA) [1,2,4], polyamide (PA) [5], and polycarbonate (PC) [6]. The material extrusion (ME) method, which is the most representative 3D printing process, has the advantages of involving simple equipment, low price, and the ability to print various composite materials, although it has the disadvantage of very low resolution and surface quality. The powder bed fusion (PBF) method, which uses a laser as a selective heat source, has excellent printing quality, although it is difficult to achieve various properties due to material limitations caused by processes characteristic of selective rapid heating. On the other hand, thermosetting polymer materials such as epoxy resins are mainly used for printing methods using ultraviolet (UV) light sources such as UV laser or digital light processing (DLP) [7–9]. Since UV energy is irradiated into the liquid resin to cause a solidification reaction, the structural precision and bonding strength between layers are excellent, although there are limitations in terms of material diversity and functionality. As such, 3D printing process using UV energy is used in various fields, such as in the aerospace industry to create complex and lightweight structures [10], in architecture to create structural models [11], in art fields for artifact replication or education [12], and in medical fields for printing of tissues

and organs [13], although there are many restrictions on its functional implementation, meaning it is limited to the production of conceptual prototypes.

Polymer-based composites and multi-material printing are being studied as new alternatives to impart various selective functionalities to 3D-printed structures [14–17]. In particular, among the various 3D printing methods, research cases using the photo-catalytic reaction method, which can lower equipment costs while maintaining high resolution and good surface quality, have been published extensively [18,19]. Among the photo-catalytic reaction methods, material jetting (MJ) is based on an inkjet structure, meaning it has advantages in terms of the printing quality and material diversity through the use of multiple nozzles [20]; however, in the MJ method, since the material is sprayed through a fine nozzle and then cured by ultraviolet light as is, if a material is used with physical properties that are difficult to control, the quality is greatly reduced [21]. In addition, if a composite material containing powder is used, abrasion and clogging of the fine nozzle may occur due to the powder; that is, since most of the composite materials used for 3D printing contain various functional powder materials, the viscosity of the resin used increases and aggregation occurs, which makes it difficult to use them in MJ 3D printing. For this reason, recently the printing of functional composite materials using photo-polymerization (PP) has been actively studied [22–25]. Among these studies, a method involving the curing of resin using a DLP projector has been widely used due to the relatively low price and high printing speed involved.

Figure 1 shows a schematic diagram of the photo-polymerization process based using a DLP projector when photochromic pigments are used as the functional powder materials. The UV-curable resin used in the photo-polymerization method is basically composed of a monomer, an oligomer, a photo-polymerization initiator, an absorber, and other components. When UV light is irradiated onto the resin, the initiator in the resin absorbs the UV energy of a specific wavelength to generate radicals or cations in order to induce polymerization, thereby forming a link between materials such as the monomers and oligomers to make a polymer [26]. At this time, the photochromic powder mixed with the composite material in this study exists in a physically dispersed state in the UV-curable resin; therefore, as a chemical photo-polymerization reaction occurs due to the ultraviolet light, a link is formed between the monomer and the oligomer and the powder is physically trapped between the linked materials, thereby making causing composite material solidification reaction. When one layer is solidified in this way, the shape of the next layer is irradiated after the Z-axis stage movement and the three-dimensional solid structure is completed via repeated additive printing.



**Figure 1.** Photo-polymerization of resin with functional powder added.

There are, however, limitations to this approach, in that it is difficult to print various materials selectively, along with the sedimentation of functional powders that occurs because printing is performed while the resin is immersed in a vat without a repetitive material supply process. Nevertheless, since the photo-polymerization method has a great advantage in terms of material diversity, various studies involving the printing of multi-composite materials are continuously being attempted. Various other methods have

been studied, including a printing method involving a rotating vat containing different resins [27], a method involving pneumatically injection and replacement of the resin in the vat [28], a method involving supply of resins using a syringe instead of a vat [29–31], and a method involving the coating of resins on thin film [32]; however, these methods have limitations in their application because the equipment involved may be excessively large compared to the size of the printed product, the zero point of the Z-axis may be shifted due to vat changes due to material switching, or powder sedimentation problems may occur.

As such, in this study, a new process and new equipment capable of printing multi-composite materials are proposed, involving a movable separator being installed in the resin vat. Since the proposed equipment does not require additional installation space, it has excellent compatibility with existing equipment, and because it is based on a single resin vat, there is no risk of shifting the origin of the Z-axis. Even when switching materials. In addition, since it is possible to generate repetitive forced flow during the 3D printing process, the problem of powder sedimentation can also be improved. Through this, the selective additive printing of multi-composite materials can be performed to evaluate various mechanical properties of the printed structure. In addition, by selective printing with appropriately rigid or flexible materials, application cases such as anisotropic structures and multi-joint grippers can be fabricated and the physical properties can be evaluated.

## 2. Experimental Details

### 2.1. Experimental Device

The equipment used in this experiment included a general 3D printer structure consisting of a FHD (1920 × 1080) DLP projector (H1180HD, Vivitek, Taipei, Taiwan), a Z-axis stage, a printing bed, and a controller, as shown in the conceptual diagram in Figure 2. In addition, a movable separator was added to a single vat to enable selective printing of two materials. As a light source, a xenon arc lamp was used, which was basically installed in a DLP projector. In this case, since the wavelength range from ultraviolet to infrared was emitted, a hot mirror (0° AOI, Edmund Optics, Barrington, NJ, USA) was used to block wavelengths above 710 nm to minimize unnecessary heat generation, which is fatal to the life of the DLP. The output power of the lamp was fixed at the level of 60% of the maximum to increase the stability and lifespan during long-term use. At this time, the output power measured with a light power meter (UIT-250, USHIO, Tokyo, Japan) from the printing surface was 3.12 mW/cm<sup>2</sup>. The resin vat was made by attaching Teflon tape with excellent release force to the bottom of an acrylic plate so that the cured resin was separated well while having excellent ultraviolet light transmission during the process. A movable separator, as shown in Figure 3, was installed so that the two materials could be selectively switched. A vehicle wiper blade rubber was attached to the edge of the separator to ensure that it had sufficient durability for repeated movement and could be easily replaced at the same time. Precision-grade LM guides were installed on both sides to allow the vat and separator to move horizontally while maintaining a constant distance. Table 1 shows the specifications for the proposed 3D printer. The thickness of each layer could be controlled from 25 to 100 μm, although it was set to 50 μm in consideration of the printing time and precision.

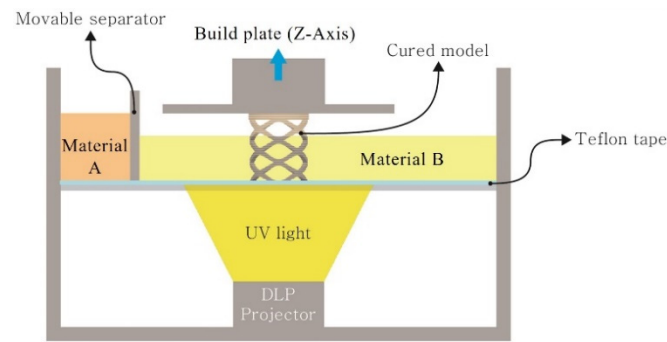


Figure 2. Conceptual diagram of the suggested printing equipment.

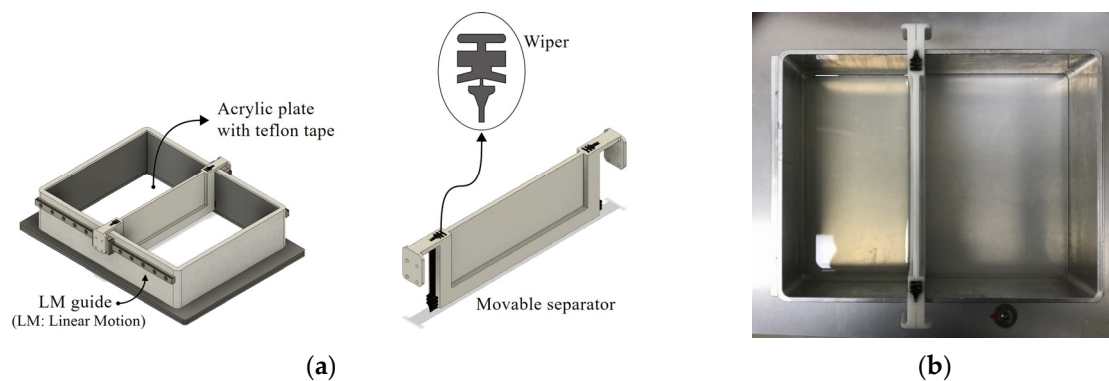


Figure 3. Vat with movable separator: (a) schematic diagram; (b) photo of the fabricated vat.

Table 1. Printing conditions for test specimen fabrication.

Variables	Values
Build size	134.4 mm × 75.6 mm × 200 mm
X-Y pixel resolution	70 μm
Curing power	3.12 mw/cm <sup>2</sup>
Layer thickness	50 μm

## 2.2. Materials

Hard (STD-clear, TINT, Gunsan, Korea) and soft (Flexible resin, XYZprinting, New Taipei, Taiwan) materials, which had significantly different mechanical properties after photo-polymerization reactions, were used to investigate the changes in the physical properties of the printed structure through selectively switched printing of multiple materials. In order to provide additional functionality, a photochromic catalyst that was able to visualize the differences without significantly changing the mechanical properties of two materials among various powders was mixed. There are two types of photochromic catalysts, dyes and pigments; most of the previous 3D printing studies have used dyes, which are completely soluble in resin, meaning there are no dispersion problems and they are easy to print; however, the dyes are mainly soluble in organic solvents, such as acetone and ethanol, as well as specific polymers (PP, PE, ABS, acrylics, etc.), so there are restrictions on the usable materials and they are very sensitive to the mixing ratio. In addition, they are chemically unstable because they are altered by the hydroxyl group (OH), so there is a limitation in using them conveniently as general-purpose materials. On the other hand, pigments are chemically stable, meaning they do not dissolve or react in the resin and the color develops by itself; however, when printing composite materials containing pigment-type photochromic powder using a general 3D printer, the printing quality is greatly reduced due to problems such as sedimentation or reduced dispersion. On the other hand, the proposed movable separator in this study can produce a continuous forced flow of resin

during the printing process, which can solve the above dispersion problems; therefore, a pigment-type photochromic powder with little influence on the material properties and excellent versatility was physically mixed with two types of commercial resins.

The pigment-type photochromic powder (C-Red and C-Yellow, Nano ENC, Ansong, Korea) used in this experiment had an average size of about 1 to 5  $\mu\text{m}$  and color expression at 280 to 382 nm of UV wavelength; therefore, in normal times, it appeared as a single material without distinguishing colors, although when irradiated with light of a specific wavelength the color changed so that the mechanical properties could be seen. For this purpose, as shown in Table 2, composite materials A and B were prepared by mixing 5 wt% of two types of photochromic powder with two types of commercial resin. Both commercial resins used in this experiment were clear-type resins, although the transparency of composite materials A and B was decreased due to the influence of the mixed photochromic pigment. As a result, the two composite materials showed a similar opaque ivory color in an environment without UV, although there was a difference in contrast. In order to determine the curing conditions for the two composite materials, as shown in Table 3, the cured depth was measured while the light irradiation time was changed in units of 1 s. The curing characteristics of the original materials were different, and as the added pigment was discolored by ultraviolet light during the printing process, it affected the photo-polymerization reaction, and thus the curability was lower than that of the original materials. In order to secure sufficient interlayer bonding strength and mechanical properties, the curing times of materials A and B were set to 2 and 3 s, respectively.

**Table 2.** Weight ratio of the composite materials.

	Material A		Material B	
	STD Resin (Hard Material)	C-Red Pigment	Flexible Resin (Soft Material)	C-Yellow Pigment
Weight ratio (%)	95	5	95	5

**Table 3.** Cured depth according to UV exposure time.

	UV Exposure Time(s)						
	1	2	3	4	5	6	7
Material A ( $\mu\text{m}$ )	60	190	230	320	360	390	420
Material B ( $\mu\text{m}$ )	-	-	111	192	271	361	436

### 2.3. Test Methods

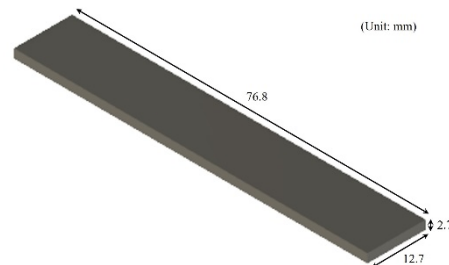
#### 2.3.1. Three-Point Bending Test

In order to measure the flexural stress using the 3-point bending test, which is widely used to measure the mechanical properties of a plate, a thin rectangular bar-shaped specimen of 76.8 mm  $\times$  12.7 mm  $\times$  2.7 mm based on the American Society for Testing and Materials (ASTM) D790 was designed, as shown in Figures 4 and S1 [33]. A micro material tester (E3000LT, Instron, Norwood, MA, USA) with a maximum static load of 2100 N and an accuracy of 0.15 N was used to measure the flexural stress. A bar specimen manufactured according to a standard test method was placed on two circular supports and a load was applied to the middle part between the supports with a round loading nose. The diameter of the support and the loading nose was  $5.0 \pm 0.1$  mm. Since the support spacing should be set between 15 and 17 times the thickness of the specimen, the depths of the beam ( $d$ ) and support span ( $L$ ) were set to 2.7 mm and 45 mm, respectively. Since a polymer based material was used, it could withstand a relatively large bending deformation; therefore, after setting the rate of straining of the outer fiber ( $Z$ ) to 0.1 mm/mm/min, the rate of crosshead motion ( $R$ ) was set as 12.5 mm/min based on Equation (1). According to ASTM, the test was carried out until the strain reached 5%, and in order to secure reliable results, all specimens were fabricated and tested 5 times each. The flexural stress ( $\sigma_f$ ) was calculated

using Equation (2) based on the obtained load value ( $P$ ). At this time, the width of the beam ( $b$ ) was 12.7 mm.

$$R = ZL^2/6d \quad (1)$$

$$\sigma_f = 3PL/2bd^2 \quad (2)$$

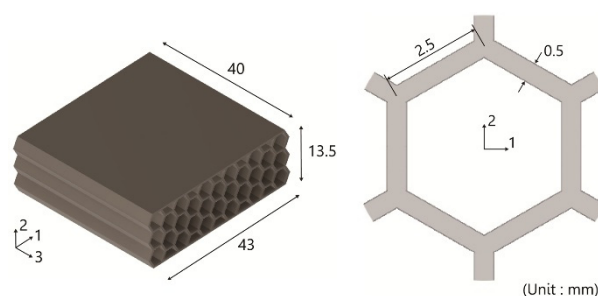


**Figure 4.** Dimensions for the 3-point bending test.

### 2.3.2. Ball Rebound Test

In order to test the degree of resilience of the printed specimen, a ball rebound test was performed based on ASTM D3574 [34]. The dimensions of the specimen were 43 mm × 40 mm × 13.5 mm based on the ASTM D3574-Test H standard, while the internal structure was designed as a complex honeycomb structure, as shown in Figures 5 and S2, in order to maximize the differences between materials and the advantages of 3D printing. The honeycomb was designed as a regular hexagonal grid structure with a side length of 2.5 mm and a shell thickness of 0.5 mm; however, when the surface of the specimen was also fabricated as a honeycomb structure, the contact surface was not uniform when the steel ball was dropped, so the bounce direction or the degree of shock absorption varied depending on the location. As such, in order to increase the reliability of the test, the surface was designed in the shape of a flat plate with a thickness of 0.5 mm. A steel ball tester suitable for ASTM D3574-Test H standard was also made. A steel ball with a diameter of  $16.03 \pm 0.2$  mm was attached to an electromagnet to allow it to fall freely from a height of 500 mm. To measure the height of the bouncing steel ball, an acrylic tube with an inner diameter of  $40 \pm 4$  mm was installed and a ruler with 1 mm units was attached. In order to eliminate the effect of the bottom surface, the specimen was fixed on the surface plate and then the steel ball tester was installed in accordance with the height of the specimen top surface. At this time, the steel ball tester was fixed to the wall so that the weight of the steel ball tester was not transferred to the specimen. To measure the rebound height, a camera capable of high-speed shooting (iPhone 7, Apple, Cupertino, CA, USA) was fixed to a tripod, and the maximum height of the steel ball was measured by recording at 720 p (HD) and 240 fps. In order to ensure the reliability, the test was performed 3 times. Based on the measured maximum rebound height, the rebound height ratio was calculated using Equation (3).

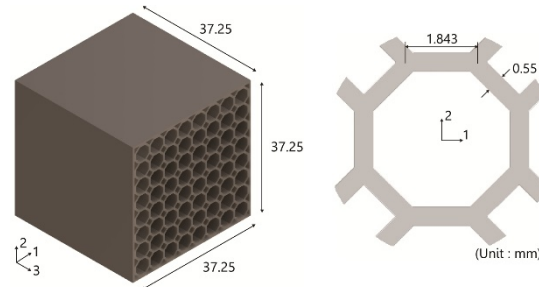
$$\text{Rebound height ratio} = \frac{\text{Maximum rebound height}}{\text{Height of drop}} \quad (3)$$



**Figure 5.** Dimensions for the ball rebound test.

### 2.3.3. Anisotropic Structure Test

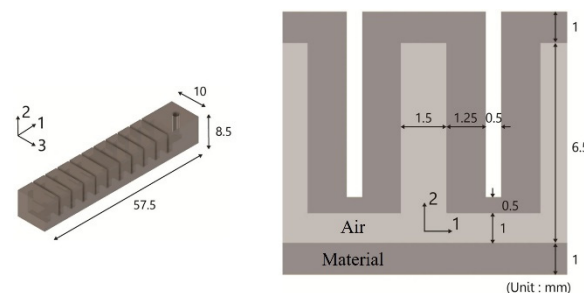
The laminar composite structure, involving continuously switched printing of two materials with a thin layer thickness, showed a new mechanical property rather than showing the properties of individual materials; however, since the printing of two materials in the macro area similarly to a half-and-half structure showed the mechanical properties of each material individually, the measured values of the impact or bending test were different depending on the test direction. Using these results, the anisotropic structure was used to change the resilience property according to the impact direction of the steel ball by switching the printing material inside the structure for each section. The specimen for the test was designed as a  $37.25 \text{ mm} \times 37.25 \text{ mm} \times 37.25 \text{ mm}$  cube with the same size as shown in Figures 6 and S3 in order to satisfy the ASTM D3574 TEST H standard and to avoid structural differences depending on the impact direction of the steel ball. As in the previous test, the surface of the cube directly contacting the steel ball was designed as a flat plate shape to reduce test errors. In order to eliminate structural differences depending on the impact direction, a regular octagonal structure with a side length of 1.843 mm and a shell thickness of 0.55 mm was continuously arranged inside the specimen.



**Figure 6.** Dimensions of the anisotropic structures.

### 2.3.4. Soft Grippers Test

The use of 3D printing is common in the fabrication of pneumatic grippers for soft robots because it is easy to print complex structures [35–37]; however, in previous studies, it was not possible to change the various behaviors of the grippers because the printing was based on a single material. Using the composite material printing process proposed in this study, it is possible to provide different selective properties for each position of the gripper, allowing for more diverse types of pneumatic gripper behavior; therefore, as shown in Figures 7 and S4, after designing the pneumatic gripper, the behavioral changes according to the pneumatic pressure were examined while changing the material for each printing position.



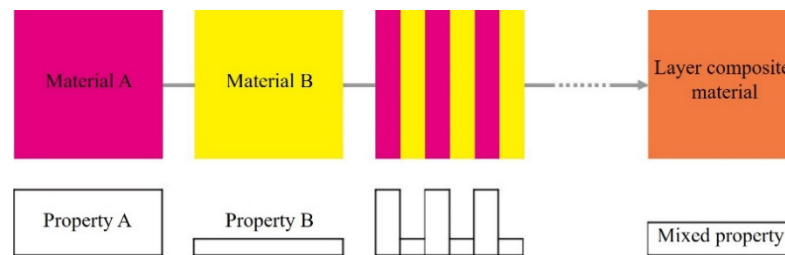
**Figure 7.** Dimensions of the soft gripper.

## 3. Results and Discussion

### 3.1. Laminar Composite Structure

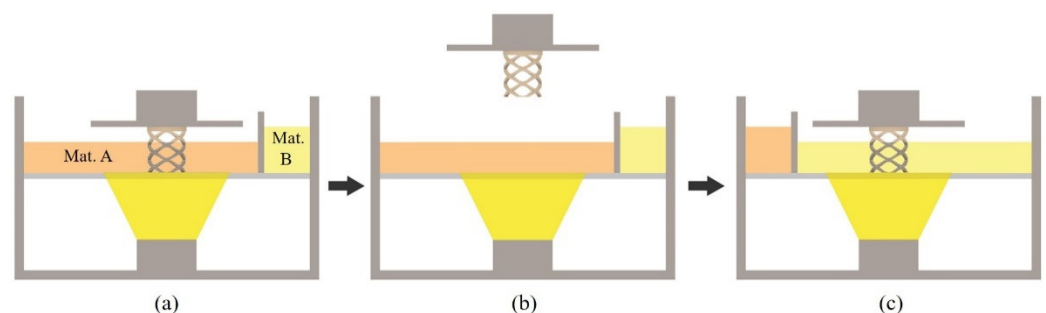
The laminar composite structure is similar to the concept of pattern recognition [38], which approaches the human perception ability as a pixel-based computer. When three

colors of light are irradiated into a local area, it appears as one color due to averaging of the color ratios. In a similar way, two or more materials with different properties can be used to create a new composite material with altered properties [39,40]; therefore, in this paper, as shown in Figure 8, a plate-reinforced composite structure was produced through selectively switched printing of two different materials. In this process, if two materials with different mechanical properties are continuously switched with a thin printing layer thickness, structures with new properties can be manufactured from a macroscopic point of view.



**Figure 8.** Layer-by-layer additive manufacturing for laminar composite structures.

A movable separator was used to selectively print two types of materials on a desired layer. As shown in Figure 9, material switching was achieved through the following process. When the printing bed was raised after the curing of one layer was completed, the movable separator pushed the existing material A out of the printing area and filled the vat with material B. Next, the printing bed descended again to cure the next layer with the switched material. At this time, since the bonding force between different materials is lower than that of the same material, immediately after changing the material, 2 s of additionally curing took place, which was longer than the basic irradiation time of the changed material [31]. The printed structure was post-processed in a UV curing machine for 1 h to secure stable properties and then used for the experiment.



**Figure 9.** Schematic diagram of the suggested process: (a) photo-polymerization of material A; (b) moving the separator for material switching; (c) photo-polymerization of material B.

### 3.2. Three-Point Bending Test

#### 3.2.1. Fabricated Specimens

As shown in Figure 10, a total of 5 types of specimens were prepared according to the material and printing method. Since the manufacturer did not provide the mechanical properties of the base resins of materials A and B, test specimens for a single material were also prepared. In addition, since materials could also be changed through complicated processes with the existing equipment, half-and-half structures were fabricated by changing the material only once, as shown in Figure 10c,d. In general, when conducting a bending test, compressive force is generated on the upper surface under load and tensile force is generated on the opposite surface. Accordingly, since the flexural stress behavior varies depending on the upper and lower positions of materials A and B, two types of



specimens were prepared in the order of material A–B and B–A, respectively. Finally, the laminar composite structure described in Section 3.1 was fabricated while continuously changing the material for each layer. As can be seen in Figure 10, the printed specimen was observed to have almost the same color in an indoor space without ultraviolet rays, although there was little difference in contrast; however, it was confirmed that different colors were shown due to the influence of the photochromic pigment present inside the material when irradiated with ultraviolet light. When material A with red pigment and material B with yellow pigment were printed with only a single composite material, this was observed according to the color of the pigment mixed in each material. For the half-and-half structures printed with different materials at half of the total thickness, the color of the material located on the top was observed. For the laminar composite structure in which the material was changed for every printed layer, a mixed color of red and yellow was observed. Through this, it was confirmed that the structures printed with a composite material mixed with photochromic pigments were able to show the differences between materials through ultraviolet irradiation.
















Structure Type	Design	UV off	UV on
(a) Material A			
(b) Material B			
(c) Half-and-half (Material A–B)			
(d) Half-and-half (Material B–A)			
(e) Laminar composite			

Figure 10. Specimens in the 3-point bending test.

### 3.2.2. Test Results

As a result of the 3-point bending test, the flexural strain and stress were obtained as shown in Figure 11. Based on ASTM, the test was carried out up to the point of flexural strain of 5%, with no fracture occurring in any of the specimens. The test was repeated 5 times for each specimen and the flexural stress at 5% flexural strain is shown in Figure 12 as the average and standard deviation. For materials A and B, which were printed with only a single composite material, the difference in mechanical properties of the base resin was very large, so the differences were about 20 times greater with flexural stress levels of 4.746 MPa and 0.228 MPa, respectively. For the half-and-half structure, in which the material was changed only once and printed with different materials for half of the total thickness, the value was slightly lower than the median value of the flexural stress of materials A and B. In addition, the flexural stress levels differed by about 25% depending on the printing order and bending direction of materials A and B. As mentioned above,

this was because the type of force received by each material varied depending on the printing order and bending direction of the materials. Accordingly, when hard material A received tensile force it showed about 25% higher flexural stress than when soft material B received tensile force. On the other hand, for the laminar composite structure in which the material was changed for each printed layer, a force of 2.326 MPa, which was similar to the median value for materials A and B, was shown regardless of the printing order or bending direction of the materials. In other words, the half-and-half structure and the laminar composite structure contained the same ratio of materials A and B, although their bending properties were different. Unlike the half-and-half structure, which was a simple bond of two plates with different properties, the laminar composite structure showed mixed properties from a macroscopic point of view due to the plate-reinforced effect caused by continuously changing the printed material for each layer over a microscopic area.

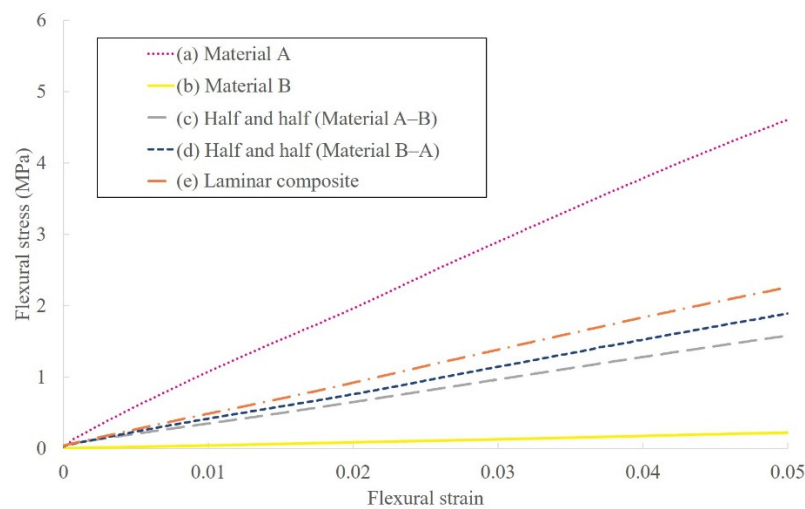


Figure 11. Flexural strain-stress graph.

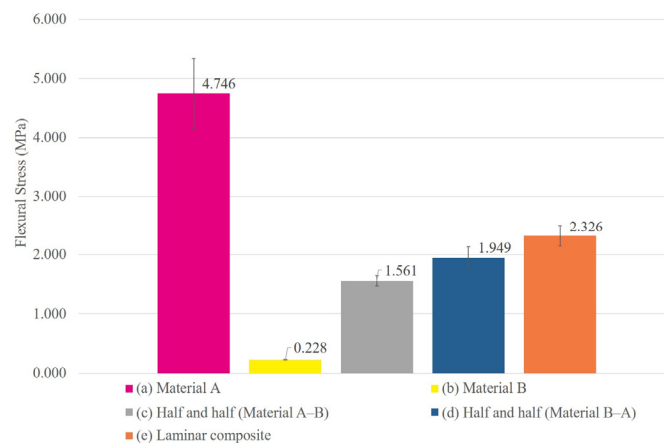


Figure 12. Average flexural stress at 5% strain.

### 3.3. Ball Rebound Test

#### 3.3.1. Fabricated Specimens

As shown in Figure 13, five types of specimens were fabricated in similar types to the 3-point bending test specimens. The test specimens were two types of specimens printed with materials A or B, two types of half-and-half structures with different surface properties in contact with the steel ball with different printing orders, and one type of laminar composite structure. Similar to the previous test, each printed specimen showed

similar colors in an indoor space without UV light, although when exposed to UV light, different colors were shown for each material by the mixed photochromic pigment.






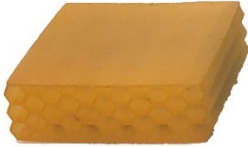






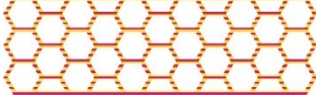
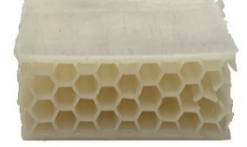

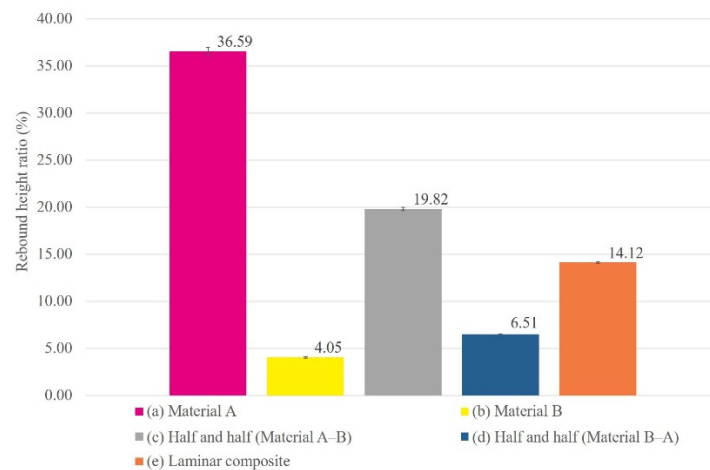
Structure Type	Design	UV off	UV on
(a) Material A			
(b) Material B			
(c) Half-and-half (Material A–B)			
(d) Half-and-half (Material B–A)			
(e) Laminar composite			

Figure 13. Specimens in the ball rebound test.

### 3.3.2. Test Results

The ball rebound test was repeated 3 times for each specimen type, with the average and standard deviation of the test results shown in Figure 14. For materials A and B, which were printed with only a single composite material, the rebound height ratios were 36.59% and 4.05%, respectively, which showed an approximate 9-fold difference due to the differences in the mechanical properties of the base resin. In particular, in this test, even for the half-and-half structure, the properties of the surface in contact with the steel ball changed significantly depending on the printing order, resulting in a difference of more than 3 times at the rebound height ratio. Although the material ratio and structure were the same, it could be seen that the case where the steel ball contacted hard material A had significantly higher resilience than the case where the steel ball contacted soft material B. Through this, it was found that the half-and-half structure behaved as if two plates with different properties were simply joined together, as in the previous 3-point bending test. On the other hand, the laminar composite structure showed similar properties to a new material through the plate-reinforced composite effect, as evidenced by having the same rebound height ratio regardless of the direction of the steel ball impact.



**Figure 14.** Average rebound height ratios.

### 3.4. Anisotropic Structures

#### 3.4.1. Fabricated Specimens

As shown in Figure 15, two types of test specimens containing either material A or B and one specimen designed to have anisotropic properties by applying a half-and-half structure were fabricated. Anisotropic structures were classified to measure resilience properties into anisotropic-1 and anisotropic-2 according to the impact direction of the steel ball, which rotated 90 degrees; that is, out of the eight sides of the regular octagon, which was the shape of the internal structure, only two sides perpendicular to the curing surface were printed with soft material B, while the other sides were printed with hard material A. The printed specimens were classified as anisotropic-1 when the ball impact test was performed at the perpendicular direction to the curing surface. When the ball impact direction was parallel to the curing plane by rotating the printed specimen by 90 degrees, this was referred to as anisotropic-2.

#### 3.4.2. Test Results

A ball rebound test was performed to evaluate the fabricated anisotropic structure. To ensure the reliability of the test, the average and standard deviation are shown in Figure 16, which were obtained after repeating the same test 3 times for each specimen type. For materials A and B, which were printed with only a single composite material, the rebound height ratios were 15.07% and 2.99%, respectively. For the anisotropic-1 specimen, only the two longitudinal axes parallel to the direction of impact of the steel ball consisted of material B and the rest consisted of material A, resulting in a rebound height ratio of 6.93%. On the other hand, for the anisotropic-2 specimen, which was subjected to the ball rebound test by rotating the same specimen by 90 degrees with respect to the printed plane, a rebound height ratio of 10.73% was shown. This was because among the regular octagonal sides, when the side parallel to the impact direction of the steel ball consisted of relatively soft material B, impact absorption was better than in other cases; therefore, it was possible to fabricate an anisotropic structure with a resilience difference of 155% depending on the impact direction during printing while selectively switching the material.

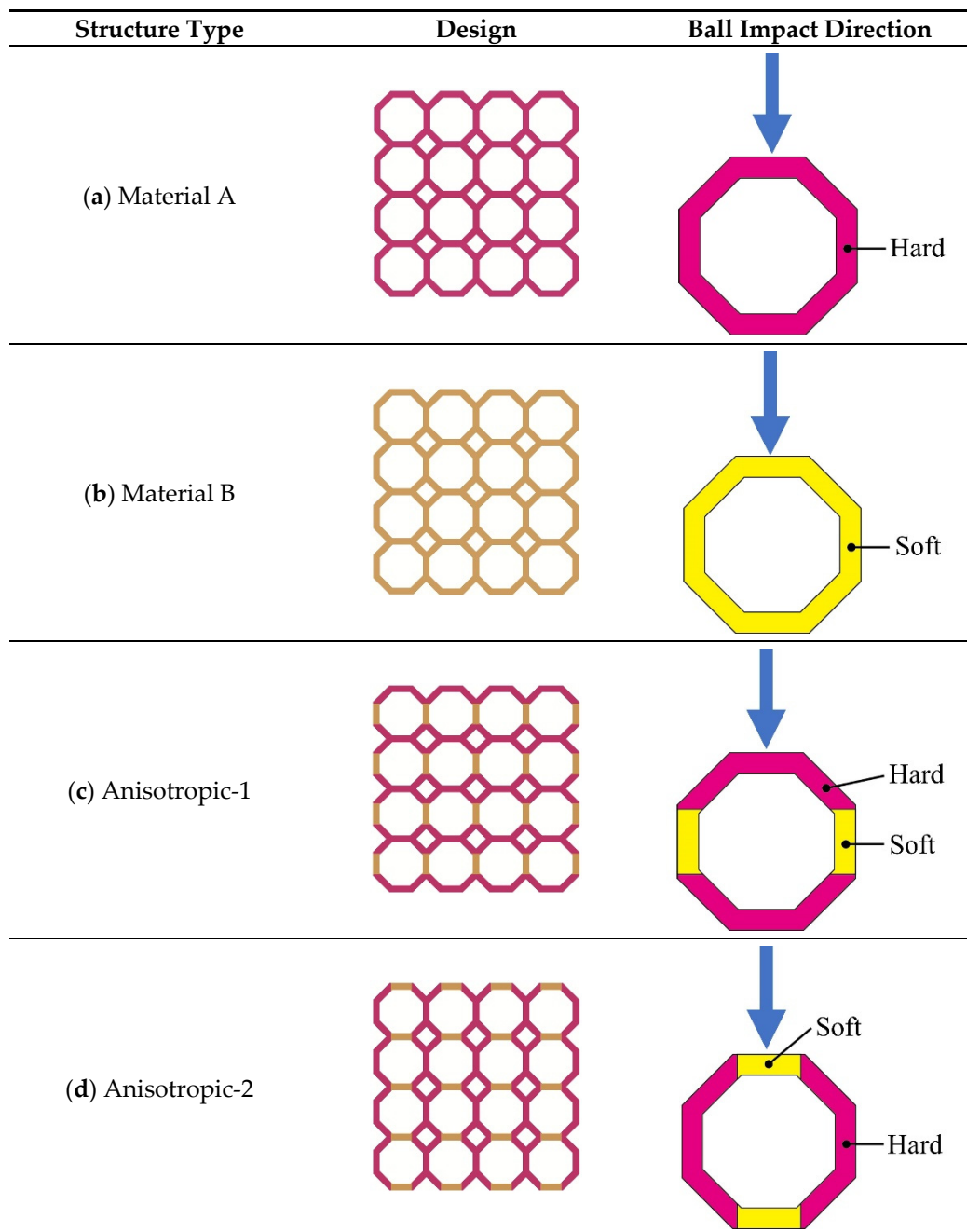
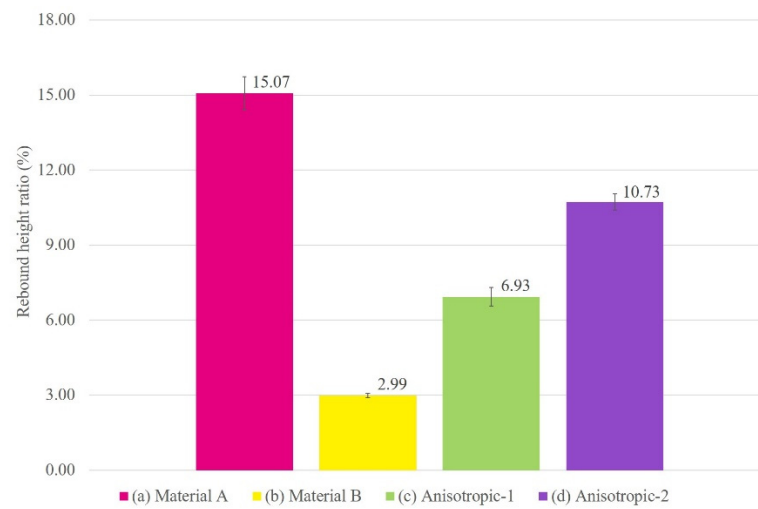


Figure 15. Specimens with different anisotropic structures.



**Figure 16.** Average rebound height ratios of the anisotropic structures.

### 3.5. Soft Grippers

#### 3.5.1. Fabricated Specimens

As shown in Figure 17, the test specimens were one type of gripper printed only with soft material B, one type of half-and-half structure gripper for selective deformation, and one type of laminar composite structure gripper designed for enhancing rigidity. Each of the printed grippers exhibited similar colors in an indoor space without UV light, although different colors were produced according to the mixed photochromic pigments when exposed to UV light.

Structure Type	Design	Pneumatic Soft Grippers under UV Light
(a) Material B		
(b) Half-and-half (Selectively flexible)		
(c) Laminar composite		

**Figure 17.** Soft gripper specimens involved in the pneumatic test.

### 3.5.2. Test Results

In order to examine the deformation behavior according to the pneumatic pressure of the fabricated gripper, a 3 mm pneumatic fitting was inserted and then connected to an air compressor. The input pneumatic pressure was changed to 75, 100, and 150 kPa using a regulator. At this time, a test was performed on a 5 mm grid scale plate to measure the radius of curvature of the deformed gripper. As shown in Figure 18, when the specimen was printed with only soft material B, the properties of the gripper were uniform over the entire area so it was deformed evenly. Additionally, as the pneumatic pressure increased, the amount of deformation increased and the radius of the curvature decreased. On the other hand, when the gripper was printed in a half-and-half structure, the mechanical properties of the gripper were different depending on the region. The hard part printed with material A showed little deformation and only the soft part printed with material B was deformed. At this time, the radius of the curvature according to the pneumatic pressure of the region containing material B where the deformation occurred was measured as being a similar value to the case where only a single material was printed in the previous test. As such, the gripper with the half-and-half structure maintained the properties of each material, enabling selective stiffness variation.

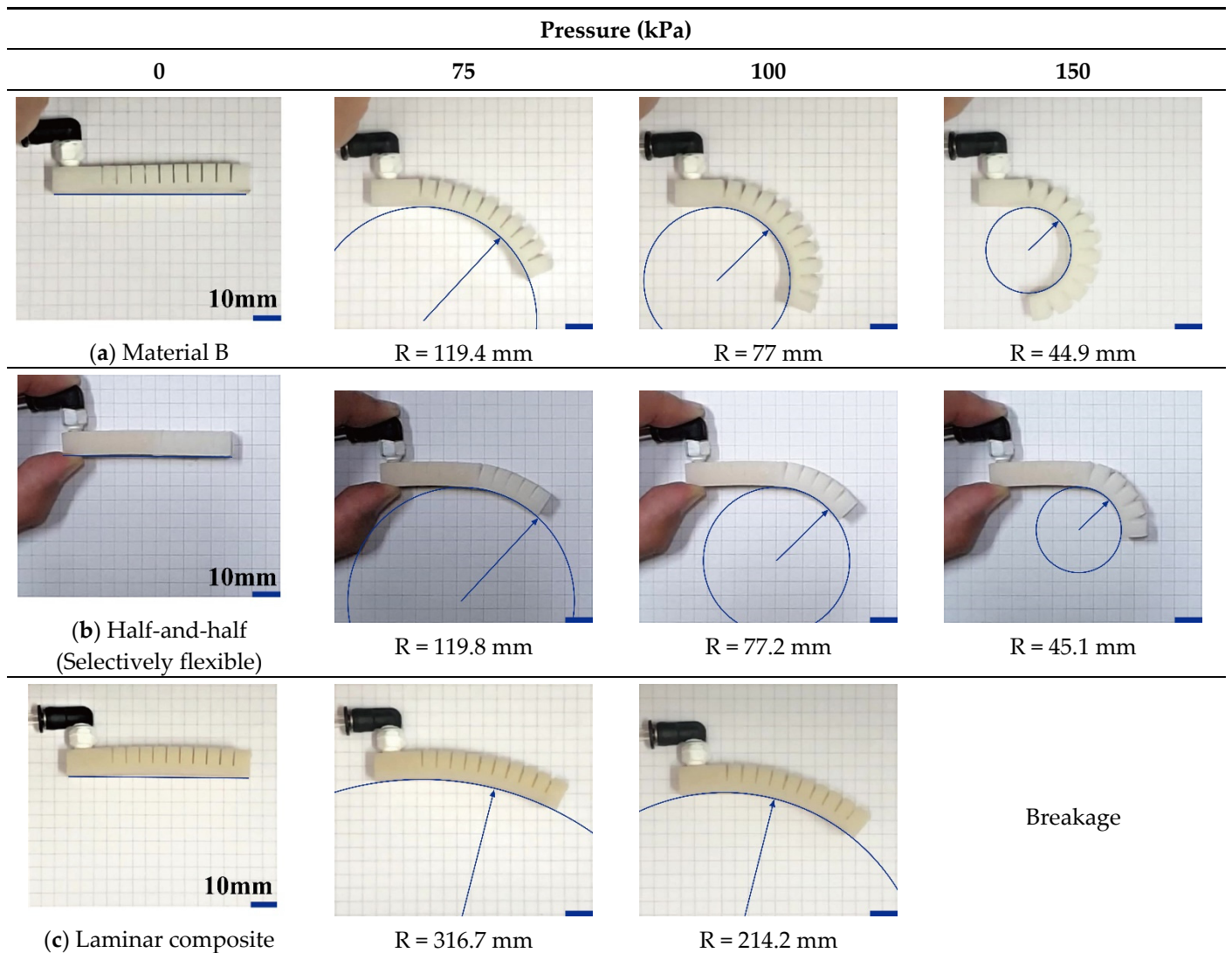


Figure 18. Deformation of soft grippers with different 3D-printed material structures in the pneumatic test.

Regarding the gripper printed with materials A and B as a laminar composite structure, the properties were uniform throughout the entire region, similarly to a new mixed material, due to the plate-reinforced effect. As such, it was deformed evenly, as in the case of printing with a single material; however, since hard material A occupied 50% of the printed layer, the mechanical strength was greatly increased and the measured radius of the curvature was relatively large compared to the other specimens. In addition, the gripper was broken at a pressure of 150 kPa due to a decrease in flexibility.

#### 4. Conclusions

In this study, a movable separator was proposed to facilitate separation between materials and dispersion of powder in order to print multi-composite materials using UV-DLP-based photo-polymerization 3D printing. The proposed system has a simpler structure and smaller size compared to the previous systems used for printing multi-materials, making it easy to install on existing equipment. In addition, the production speed and printing precision are also improved. In other words, if the proposed method is used, it is possible to change materials quickly without alignment errors, so it is possible to implement various types of printing based on multi-composite materials; therefore, two types of composite materials were prepared by mixing a photochromic powder with two resins with different mechanical properties, which were classified into a single material structure, a half-and-half structure, and a laminar composite structure according to the printed form. As a result of the bending test and rebound test on the fabricated specimen, when two materials with different mechanical properties were printed with a laminar composite structure, the mechanical properties showed intermediate values between the two materials. In other words, when two materials with different mechanical properties were continuously cross-printed in the micro region with a thin layer thickness, the structure resembled a plate-reinforced composite structure, making it possible to fabricate structures with new properties from a macroscopic point of view. On the other hand, in the half-and-half structure, since the material was changed in the macro area, the mechanical properties of each material were maintained; therefore, the mechanical properties were different for each printing area. Using these properties, it was possible to fabricate anisotropic structures and soft grippers capable of selective deformation. In addition, since composite materials mixed with photochromic powder responding to UV light were used, the mechanical strengths of the structures could be visually confirmed. Through this, it was possible to fabricate 3D structures with various strengths and functionalities through selective printing of multi-composite materials based on the proposed movable separator. This method of multi-composite material 3D printing can be combined with the design for additive manufacturing (DFAM) approach to further maximize functionality and versatility.

**Supplementary Materials:** The following are available online at <https://www.mdpi.com/article/10.3390/app11188545/s1>, Figure S1: STL image for the 3-point bending test, Figure S2: STL image for the ball rebound test, Figure S3: STL image of the anisotropic structures, Figure S4: STL image of the soft gripper.

**Author Contributions:** Conceptualization, M.-S.P.; methodology, S.-R.H.; investigation, S.-R.H. and M.-S.P.; writing—original draft preparation, S.-R.H. and M.-S.P.; writing—review and editing, M.-S.P.; supervision, M.-S.P.; project administration, M.-S.P.; funding acquisition, M.-S.P. All authors have read and agreed to the published version of the manuscript.

**Funding:** This research was supported by Basic Science Research Program through the National Research Foundation of Korea (NRF) funded by the Ministry of Science and ICT (MSIT) (no. NRF-2020R1A2C1102556).

**Institutional Review Board Statement:** Not applicable.

**Informed Consent Statement:** Not applicable.

**Data Availability Statement:** Not applicable.



**Conflicts of Interest:** The authors declare no conflict of interest. The funders had no role in the design of the study; in the collection, analyses, or interpretation of data; in the writing of the manuscript, or in the decision to publish the results.

## References

1. Tymrak, B.M.; Kreiger, M.; Pearce, J.M. Mechanical properties of components fabricated with open-source 3-D printers under realistic environmental conditions. *Mater. Des.* **2014**, *58*, 242–246. [[CrossRef](#)]
2. Tran, P.; Ngo, T.D.; Ghazlan, A.; Hui, D. Bimaterial 3D printing and numerical analysis of bio-inspired composite structures under in-plane and transverse loadings. *Compos. Part B Eng.* **2017**, *108*, 210–223. [[CrossRef](#)]
3. Sun, Q.; Rizvi, G.M.; Bellehumeur, C.T.; Gu, P. Effect of processing conditions on the bonding quality of FDM polymer filaments. *Rapid Prototyp. J.* **2008**, *14*, 72–80. [[CrossRef](#)]
4. Melnikova, R.; Ehrmann, A.; Finsterbusch, K. 3D printing of textile-based structures by Fused Deposition Modelling (FDM) with different polymer materials. In Proceedings of the 2014 Global Conference on Polymer and Composite Materials (PCM 2014), Ningbo, China, 27–29 May 2014; Institute of Physics Publishing: Bristol, England, 2014; Volume 62, p. 012018.
5. Caulfield, B.; McHugh, P.E.; Lohfeld, S. Dependence of mechanical properties of polyamide components on build parameters in the SLS process. *J. Mater. Process. Technol.* **2007**, *182*, 477–488. [[CrossRef](#)]
6. Garcia, C.R.; Correa, J.; Espalin, D.; Barton, J.H.; Rumpf, R.C.; Wicker, R.; Gonzalez, V. 3D printing of anisotropic metamaterials. *Prog. Electromagn. Res. Lett.* **2012**, *34*, 75–82. [[CrossRef](#)]
7. Gu, H.; Ma, C.; Gu, J.; Guo, J.; Yan, X.; Huang, J.; Zhang, Q.; Guo, Z. An overview of multifunctional epoxy nanocomposites. *J. Mater. Chem. C* **2016**, *4*, 5890–5906. [[CrossRef](#)]
8. Gu, J.; Yang, X.; Lv, Z.; Li, N.; Liang, C.; Zhang, Q. Functionalized graphite nanoplatelets/epoxy resin nanocomposites with high thermal conductivity. *Int. J. Heat Mass Transf.* **2016**, *92*, 15–22. [[CrossRef](#)]
9. Dou, J.; Zhang, Q.; Ma, M.; Gu, J. Fast fabrication of epoxy-functionalized magnetic polymer core-shell microspheres using glycidyl methacrylate as monomer via photo-initiated miniemulsion polymerization. *J. Magn. Magn. Mater.* **2012**, *324*, 3078–3082. [[CrossRef](#)]
10. Kroll, E.; Artzi, D. Enhancing aerospace engineering students' learning with 3D printing wind-tunnel models. *Rapid Prototyp. J.* **2011**, *17*, 393–402. [[CrossRef](#)]
11. Wong, K.V.; Hernandez, A. A Review of Additive Manufacturing. *ISRN Mech. Eng.* **2012**, *2012*, 1–10. [[CrossRef](#)]
12. Short, D.B. Use of 3D printing by museums: Educational exhibits, artifact education, and artifact restoration. *3D Print. Addit. Manuf.* **2015**, *2*, 209–215. [[CrossRef](#)]
13. Murphy, S.V.; Atala, A. 3D bioprinting of tissues and organs. *Nat. Biotechnol.* **2014**, *32*, 773–785. [[CrossRef](#)] [[PubMed](#)]
14. Wang, X.; Jiang, M.; Zhou, Z.; Gou, J.; Hui, D. 3D printing of polymer matrix composites: A review and prospective. *Compos. Part B Eng.* **2017**, *110*, 442–458. [[CrossRef](#)]
15. Shin, I.J.; Park, M.S. Direct Conductive Patterning on 3D Printed Structure Using Laser. *Phys. Status Solidi* **2018**, *215*, 1700597. [[CrossRef](#)]
16. Shin, I.; Park, M. 3D printed conductive patterns based on laser irradiation. *Phys. Status Solidi Appl. Mater. Sci.* **2017**, *214*. [[CrossRef](#)]
17. Lee, S.; Shin, C.; Jung, M.; Park, M. Property Analysis of Multi-Material Specimen based on ME Type 3D Printer. *J. Korean Soc. Precis. Eng.* **2020**, *37*, 231–238. [[CrossRef](#)]
18. Choi, S.; Park, M. Fabrication of Conductive Patterns on 3D Printed Structure Using Photo-Polymerization Technology. *Phys. Status Solidi* **2019**, *216*, 1801017. [[CrossRef](#)]
19. Mei, H.; Huang, W.; Liu, H.; Pan, L.; Cheng, L. 3D printed carbon-ceramic structures for enhancing photocatalytic properties. *Ceram. Int.* **2019**, *45*, 15223–15229. [[CrossRef](#)]
20. Tsai, M.J.; Mei, C.W.; Cheng, Y.L.; Chen, F.; Hu, Z.Y.; Huang, K.C. A study of a material jetting based color 3d printing system by using multiple piezoelectric heads. In Proceedings of the 2017 International Conference on Machine Learning and Cybernetics, ICMLC, Ningbo, China, 9–12 July 2017; Volume 2, pp. 664–669.
21. He, Z.; Shao, Z.; Wang, Q.; Zhong, W.; Tao, X. Experimental study of cavitating flow inside vertical multi-hole nozzles with different length-diameter ratios using diesel and biodiesel. *Exp. Therm. Fluid Sci.* **2015**, *60*, 252–262. [[CrossRef](#)]
22. Cramer, N.B.; Stansbury, J.W.; Bowman, C.N. Recent advances and developments in composite dental restorative materials. *J. Dental Res.* **2011**, *90*, 402–416. [[CrossRef](#)]
23. Song, S.Y.; Park, M.S.; Lee, D.; Lee, J.W.; Yun, J.S. Optimization and characterization of high-viscosity ZrO<sub>2</sub> ceramic nanocomposite resins for supportless stereolithography. *Mater. Des.* **2019**, *180*. [[CrossRef](#)]
24. Song, S.Y.; Park, M.S.; Lee, J.W.; Yun, J.S. Improvement of dispersion stability and 3D-printing characteristics of ceramics in photopolymers by controlling the coating thickness of silane coupling agents. *Mater. Chem. Phys.* **2018**, *216*, 446–453. [[CrossRef](#)]
25. Song, S.Y.; Park, M.S.; Lee, J.W.; Yun, J.S. A study on the rheological and mechanical properties of photo-curable ceramic/polymer composites with different silane coupling agents for SLA 3D printing technology. *Nanomaterials* **2018**, *8*, 93. [[CrossRef](#)]
26. Phillips, R. Photopolymerization. *J. Photochem.* **1984**, *25*, 79–82. [[CrossRef](#)]
27. Choi, J.W.; Kim, H.C.; Wicker, R. Multi-material stereolithography. *J. Mater. Process. Technol.* **2011**, *211*, 318–328. [[CrossRef](#)]

28. Han, D.; Yang, C.; Fang, N.X.; Lee, H. Rapid multi-material 3D printing with projection micro-stereolithography using dynamic fluidic control. *Addit. Manuf.* **2019**, *27*, 606–615. [[CrossRef](#)]
29. Li, V.C.F.; Kuang, X.; Hamel, C.M.; Roach, D.; Deng, Y.; Qi, H.J. Cellulose nanocrystals support material for 3D printing complexly shaped structures via multi-materials-multi-methods printing. *Addit. Manuf.* **2019**, *28*, 14–22. [[CrossRef](#)]
30. Emon, M.O.F.; Alkadi, F.; Philip, D.G.; Kim, D.H.; Lee, K.C.; Choi, J.W. Multi-material 3D printing of a soft pressure sensor. *Addit. Manuf.* **2019**, *28*, 629–638. [[CrossRef](#)]
31. Hwang, S.; Lee, J.; Lee, S.; Hong, D.; Park, M. Development of DLP 3D Printer with Multiple Composite Materials. *J. Korean Soc. Precis. Eng.* **2020**, *37*, 381–388. [[CrossRef](#)]
32. Gyak, K.W.; Vishwakarma, N.K.; Hwang, Y.H.; Kim, J.; Yun, H.S.; Kim, D.P. 3D-printed monolithic SiCN ceramic microreactors from a photocurable preceramic resin for the high temperature ammonia cracking process. *React. Chem. Eng.* **2019**, *4*, 1393–1399. [[CrossRef](#)]
33. D20-Committee. *Standard Test Methods for Flexural Properties of Unreinforced and Reinforced Plastics and Electrical Insulating Materials*(ASTM D790-17); ASTM International: West Conshohocken, PA, USA, 2017.
34. D20-Committee. *Standard Test Methods for Flexible Cellular Materials—Slab, Bonded, and Molded Urethane Foams*(ASTM D3574-01); ASTM International: West Conshohocken, PA, USA, 2001.
35. Ge, L.; Dong, L.; Wang, D.; Ge, Q.; Gu, G. A digital light processing 3D printer for fast and high-precision fabrication of soft pneumatic actuators. *Sens. Actuators A Phys.* **2018**, *273*, 285–292. [[CrossRef](#)]
36. Ding, L.; Dai, N.; Mu, X.; Xie, S.; Fan, X.; Li, D.; Cheng, X. Design of soft multi-material pneumatic actuators based on principal strain field. *Mater. Des.* **2019**, *182*, 108000. [[CrossRef](#)]
37. Herianto; Irawan, W.; Ritonga, A.S.; Prastowo, A. Design and fabrication in the loop of soft pneumatic actuators using fused deposition modelling. *Sens. Actuators A Phys.* **2019**, *298*, 111556. [[CrossRef](#)]
38. Yang, C.N.; Chen, T.S. Colored visual cryptography scheme based on additive color mixing. *Pattern Recognit.* **2008**, *41*, 3114–3129. [[CrossRef](#)]
39. Udupa, G.; Rao, S.S.; Gangadharan, K.V. Functionally Graded Composite Materials: An Overview. *Procedia Mater. Sci.* **2014**, *5*, 1291–1299. [[CrossRef](#)]
40. Correia, V.M.F.; Madeira, J.F.A.; Araújo, A.L.; Soares, C.M.M. Multiobjective optimization of functionally graded material plates with thermo-mechanical loading. *Compos. Struct.* **2019**, *207*, 845–857. [[CrossRef](#)]